The High Resolution Aeronautical Multipath Navigation Channel

Alexander Steingass, German Aerospace Center DLR
Andreas Lehner, German Aerospace Center DLR
Fernando Pérez-Fontán, University of Vigo, Spain
Erwin Kubista, Joanneum Research, Austria
Maria Jesús Martín, University of Vigo, Spain
and Bertram Arbesser-Rastburg, European Space Agency, The Netherlands

BIOGRAPHY

Alexander Steingass was born in Mettmann, Germany in 1969. He received his Dipl. Ing. diploma in Electrical Engineering in 1997 (University of Ulm, Germany). Since then he has been a research scientist at the German Aerospace Centre DLR - Institute of Communications and Navigation. He has been involved in several projects in the area of satellite navigation and location dependent mobile services. In 2002 he was promoted Dr. Ing. at the University of Essen.
Homepage: http://www.dlr.de/kn/kn-s/steingass
Email: alexander.steingass@dlr.de

Andreas Lehner was born in Gmunden, Austria in 1973. He received his diploma engineer degree in mechatronics from the university of Linz in 2001. Since then he has been a research scientist at the German Aerospace centre DLR.
Homepage: http://www.dlr.de/kn/kn-s/lehner
Email: andreas.lehner@dlr.de

Fernando Pérez-Fontán, was born in Vilagarcía de Arousa, Spain. He received a Telecommunications Engineering degree and a PhD from the Polytechnic University of Madrid in 1982 and 1992. He has been with the Telecommunications Engineering School of Vigo University since 1988, where he currently is a full professor at the Department of Signal Theory and Communications.

Erwin Kubista received the Dipl. Ing. degree in Telecommunications and Electronic Engineering from the Technical University of Graz, Austria, in 1985. He is with Joanneum Research, where he has been managing a number of projects dealing with mobile and fixed satellite wave propagation carried out under ESA and EU contracts.

María Jesús Martín, was born in Vigo, Spain. She obtained her Telecommunications Engineering degree from Vigo University in 2001. She has been involved in several Galileo projects doing deterministic and statistical modeling of the navigation propagation channel.

Bertram Arbesser-Rastburg was born in Austria. He received the DipI.-Ing. degree in electrical engineering from the Technical University of Graz, Graz, Austria, in 1980. In 1988, he joined the European Space Agency. Since 1989, he has been Head of the Wave Interaction and Propagation Section at the European Space Agency/European Space Technology Center (ESA/ESTEC), Noordwijk, The Netherlands. His research activities include propagation effects relevant to fixed, mobile, and navigation satellite systems as well as direct and indirect models of microwave interaction with the Earth's surface and the atmosphere for active and passive remote-sensing instruments.

ABSTRACT

In this paper we discuss the results of a measurement campaign investigating the environment of satellite navigation receivers for aeronautical applications, where reflections on the plane as well as from the ground and from buildings at airports decrease the accuracy of the positioning.

INTRODUCTION

Along with the development of GALILEO it became necessary to improve the knowledge about the aeronautical channel. Especially the power, the origin and the delay of the reflections at the aircraft structure were a main topic in the scientific discussions. During this exchange of opinions the lack of information concerning the bandwidth of the reflections became obvious. For that reason the European Space Agency

(ESA) commissioned a contract about a measurement campaign on this issue in autumn 2002 to a research consortium, consisting of Joanneum Research (Austria), University of Vigo (Spain) and the German Aerospace Centre (Germany).
Due to the high bandwidth of the signal, a navigation receiver is able to mitigate many reflections. Only those reflections which arrive shorter than the chip duration mainly contribute to the positioning error [5]. This nature of the system made it necessary to measure the channel with an extremely high bandwidth of 100 MHz which results in a very high time resolution of 20 ns. Using a super-resolution algorithm we have been able to reach a resolution down to 1 ns.
One of the most urgent questions of the GALILEO project was the confirmation or refutation of the aeronautical channel model being defined in the ESA signal design and transmission study (ESA-SDS [1]):

Let h(t,τ) be the impulse response of the channel model. Then h(t,τ) is given by

$$h(t,t) = 1 + \sum_{i=1}^{3} \sqrt{P_i} \cdot n_i(t) \cdot d(t - t_i)$$

where P_i is the Echo Power of the i^{th} path. The signal $n_i(t)$ is a noise signal with Power 1, and a power spectral density

$$N(f) = \begin{cases} 0 & \forall f < -B/2 \\ 1/B & \forall -B/2 < f < B/2 \\ 0 & \forall f > B/2 \end{cases}$$

The defined parameters of this model are given in the following table.

Path Nr.	Name	Delay	Relative Power	Doppler Bandwidth
1	Refractive Comp.	0 ns	-10 dB	1 Hz
2	Refractive Comp.	44 ns	-6 dB	1 Hz
3	Refractive Comp.	960 ns	-20 dB	420 Hz

Table 1 Parameters of the ESA-SDS Model

The characteristic of this model is a direct path with a refractive component (Path #1), an extremely strong echo on the wing that is changing extremely slow (Path #2), and a quickly changing ground echo (Path #3). Please note that the path #2 is the most critical one due to the high power on the one hand and the low bandwidth on the other hand, which is passing the receivers loop filter unaffected [2].

The motivation for this measurement project was to prove or refute this channel model.

MEASUREMENT

The most important scenario for this channel type is the final approach of the airplane prior to landing. In the depicted experiment we used an aircraft (Pilatus Porter) as the transmitting platform (**Figure 1**) with an installed helix, hemispherical antenna transmitting a signal on 1,95 GHz using a bandwidth of 100 MHz. The receiver was mounted in the 25m span experimental jet VFW 614 (ATTAS) approaching Thalerhof airport of Graz/Austria by a standard ILS approach. These results were expected to be used to achieve knowledge about the time progression of the channel impulse response.

To gain statistically relevant data in terms of azimuth and elevation of the incoming signal, in a second step a helicopter as transmitter circled the parked VFW 614 while the reflections on the plane were measured. To allow an extension of the measurement results to larger aircrafts the ground measurements were repeated with an Airbus A340 (**Figure 2**).

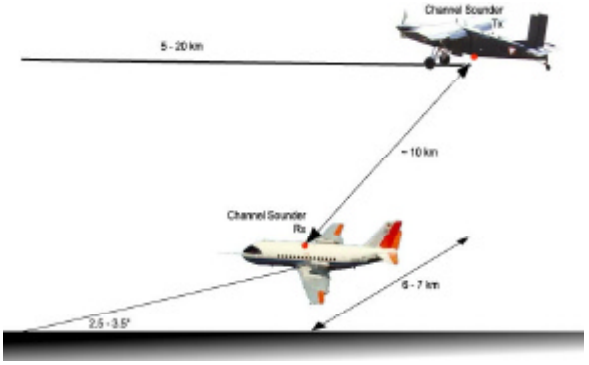

Figure 1: Measurement scenario of the Final approach

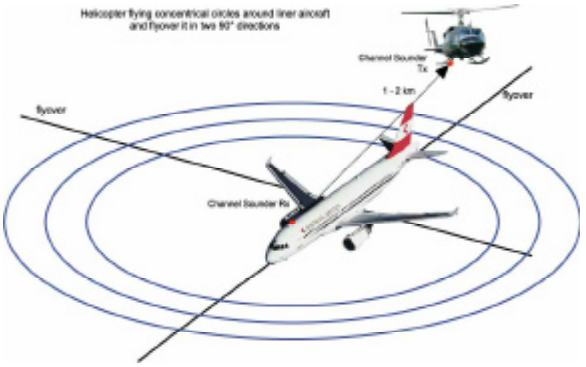

Figure 2: Plane on ground measurement

To evaluate the measurement, the raw data was post processed by using the super resolution algorithm ISIS that was provided by Elektrobit/Switzerland. This algorithm estimates the reflections in a higher

resolved time grid than the measurement bandwidth of 100 MHz would allow [3]. The timing quantisation of ISIS had been set to 0.1 ns. Pre-tests had shown that an accuracy of 1 ns in echo timing error is achievable which results in an equivalent observation bandwidth of 1 GHz. Such a bandwidth would have been necessary to provide this timing accuracy. The output of the algorithm are discrete reflection estimates characterised by: co-polar power, cross-polar-power, delay, phase, Doppler, azimuth and elevation. For the evaluation of the results the ISIS Dirac-impulses must be combined to an impulse response as if an ideal omni-directional circular polarised antenna had been used.

We name t_i the delay of the i-th path, j_i its phase and A_i the co-polar-amplitude. The theoretical observation bandwidth B had been selected to 1 GHz. Then the interpolated impulse response of the ISIS data is given by:

$$s(t,t) = \sum_i A_i \cdot \exp(jj_i) \cdot si\left(\frac{t - t_i}{B}\right)$$

where

$$si(x) = \frac{\sin(x)}{x}$$

This impulse response is plotted in **Figure 3**. The impulse response had been cyclic shifted so that the maximum of the interpolated impulse response s(t,τ) is at 0 ns.

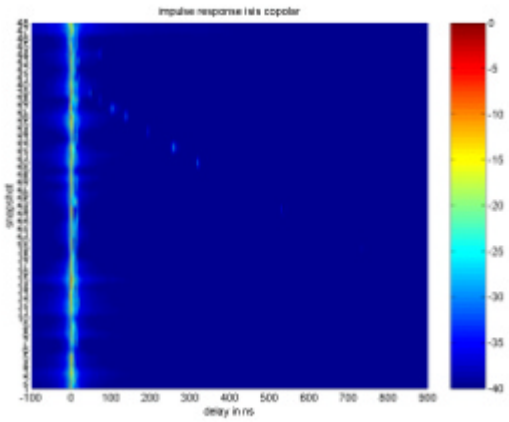

Figure 3: Channel impulse response of the final approach in a large time scale

This means the direct signal LOS (line of sight) can be seen at 0 ns delay. The y-axis shows the consecutive number of snapshot which in other words shows the progress in time of the measurement.

For the modelling we only used the co-polar component of the received signal.

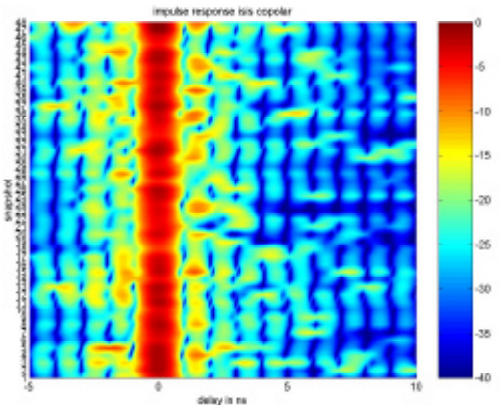

Figure 4: Measured impulse response – short time scale

For a further evaluation of the data we created plots showing the angle of arrival as well as the power of the incoming paths which is displayed in the angle of arrival (AOA) figure.

Figure 5 shows all detected rays during a final approach seen from the receiver antenna. Clusters indicate the direct signal, a reflection zone on the fuselage and a ground reflection. The black lines are edges of the airplanes structure, indicating e.g. the wings, engines and fuselage.

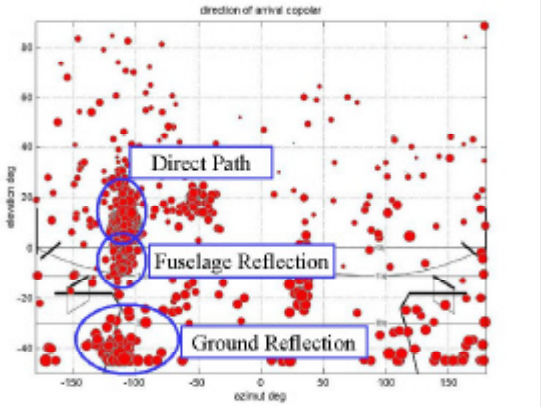

Figure 5: Angle of arrival – Dot size indicates the echo power.

Physical Optics (PO) Simulation

To verify the measurements we built a 3D model of the aircrafts and used ray tracing techniques to simulate the propagation situation.

Physical optics (PO) techniques are more general than geometrical optics (GO), because the PO equations for the scattered field from an electrical conducting body reduce to the equations of geometrical optics in the high-frequency limit.

Therefore we chose this method for the aircraft simulations.
PO assumes that the field at the surface of the scattering body is the GO surface field at each point on the illuminated side of the scatterer. The scattering takes place as if there were an infinite tangent plane at that point, while over the shadowed regions of the scatterer the field at the surface is zero [4].

For a perfectly conducting body, the assumed PO surface current is given by

$$\vec{J}_{\mathrm{PO}} = \begin{cases} \hat{n} \times \hat{H}_{Tot} & \text{in the illuminated region} \\ 0 & \text{in the shadowedregion} \end{cases}$$

with $\hat{n}$ the unit normal vector from the scattering surface.

From image theory, the tangential components of $\vec{H}$ at a perfect electrical conductor are given by

$$\vec{J}_{\mathrm{PO}} = 2\left(\hat{n} \times \hat{H}_{Incident}\right)$$

that is, it is twice the amount from the same source when the conducting scatterer is replaced by equivalent currents in free space.

For far field conditions, the PO scattered field is given by the integral

$$\vec{H}_{Scattered} \approx \frac{j\,ß}{4p\,r} e^{-j ß r} \iint_{\text{Lit surface}} (\vec{J} \times \hat{r}) e^{j ß \hat{r} \cdot \vec{r}'} ds'$$

where r is the distance from the origin to the observation point and r' is the distance from the origin to the surface point. In order to apply the above integral, the lit part of the scattering is split into small triangular patches to approximate the curved surface of the aircraft. **Figure 6** illustrates this approach. The contributions from each patch will be a delta on the channel impulse response and power delay profile.

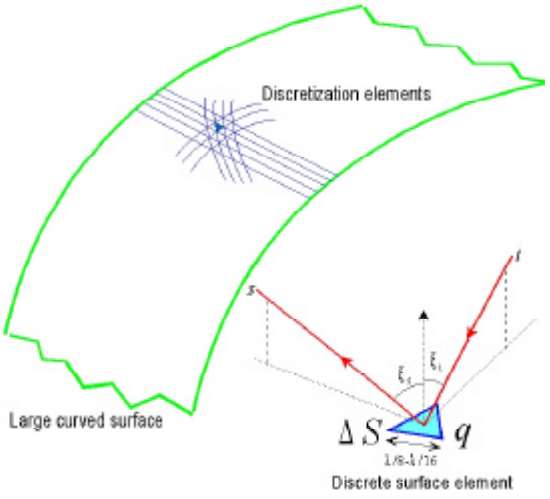

Figure 6: Physical Optics Model used for the aircraft simulations.

To generate a time series out of these static simulations we used the roll, pitch and jaw angles being recorded during the measurement. By turning the 3D model into the appropriate direction we recalculated the propagation conditions for every time instance. The A340 aircraft was simulated by using low pass filtered flight data. The result is shown in **Figure 9**.

DIRECT PATH

The existence of the direct path in the selected scenario is obvious. In **Figure 5** the direct path can be seen at azimuth = -120°, elevation = 15° which correspond directly to the transmission position.
We also can see the direct path at 0 ns delay in **Figure 4**. This path is affected by a strong modulation which seems to have a Rician distribution character. Bearing in mind that the time distance between two snapshots is 1.25 - 5 s, it can be assumed that the Doppler bandwidth of the fading process is quite small. We modelled this process according to the simulation results presented in the following chapter.

WING REFLECTION

According to Table 1 the inventors of the ESA-SDS Model expected a strong reflection from the wings. We had been very surprised that we were not able to find any wing reflection in the measurement, neither **Figure 4** nor **Figure 5** showed a hint to this reflection type. For this reason we used the physical optics model to determine the expected reflection power. The result of this simulation was a surprise: The power of the wing reflection was around –35 dB (see **Figure 8** (ATTAS) at around 40-50 ns and **Figure 9** (A 340) at 50-80 ns). This explains why we were not able to identify this reflection. This extremely low power level made clear that from no relevant error contribution can result from the wing. For this reason we decided not to model this reflection type.

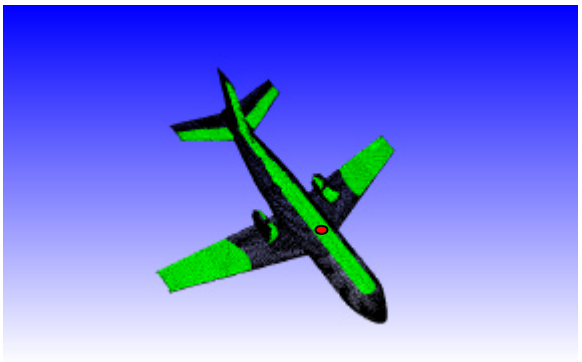

Figure 7: 3D model ATTAS. Green surfaces are visible from the antenna (red dot).

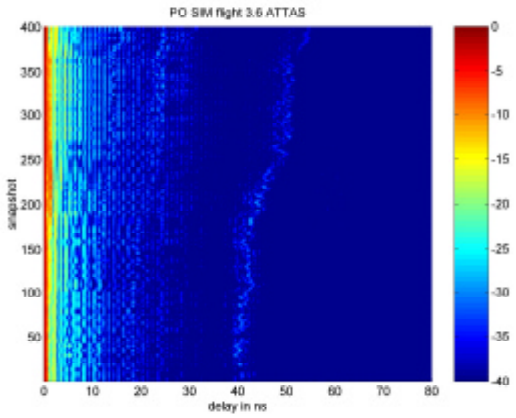

Figure 8: PO Simulation ATTAS – time series

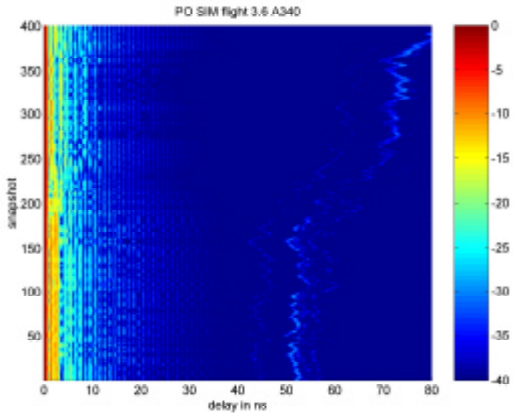

Figure 9: PO Simulation Airbus A340 - time series

FUSELAGE REFLECTION

Examinations of the impulse response plot (**Figure 4**) and AOA (**Figure 5**) plot shows that there is a quite strong reflection very close to the LOS signal at approximately 1-2 ns delay with a certain modulation on it. This is most easily seen in **Figure 10**, which is a detail of **Figure 3**.

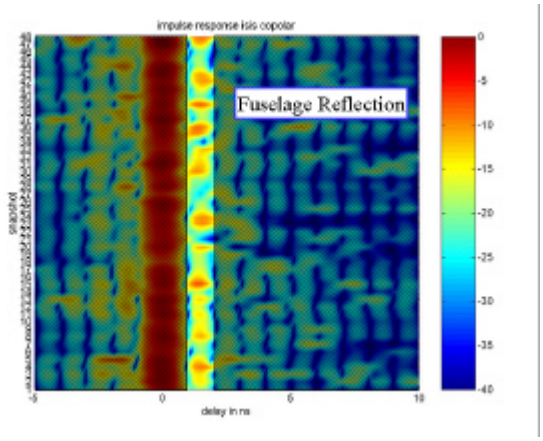

Figure 10: Measured impulse response

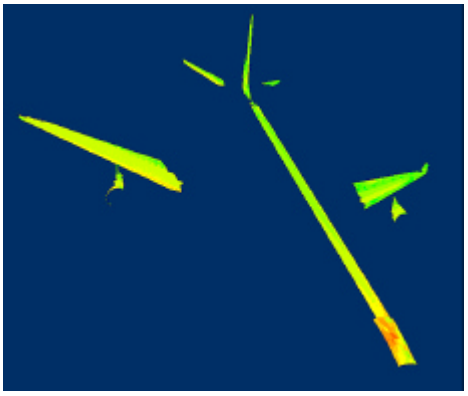

Figure 11: PO simulation of the A340. The colour indicates the strength of power contribution to the impulse response (red areas contribute a lot).

The center of the reflection area is located approximately at an elevation of -10 degrees. This position is just below the receiver antenna on the fuselage. Therefore we will call this reflection the “fuselage echo”. The power of this echo is estimated to –14.2 dB. Again, having in mind the timing grid, we assume the Doppler bandwidth of this process also to be below 0.1 Hz.

To verify the existence of a fuselage reflection we performed a PO simulation. **Figure 11** is showing the result. In this scenario the A340 was illuminated from the left side and an elevation of 15 degrees. The colour indicates the power received from the respective reflection areas. There the fuselage echo can clearly be seen as an orange spot close to the antenna on top of the cockpit.

Further trials to find another reflection were carried out. On looking carefully on the plots, another reflection could be assumed at approximately 2 - 4 ns. Under closer scrutiny we figured that these estimated rays are often coming from “nowhere in the sky” or from always changing directions. Therefore we are not able to identify a reflection in this delay range. All the other reflections shown in the figures cannot be associated to a distinguished part of the airplane. That’s why we assume that these “spots” are artefacts or false estimates of the ISIS algorithm. This is the same case for longer delayed reflections. In order to prove this assumption we took a closer look on the circular flight data. Again no clear echo could be found caused by the airplane structure. The non-existence of another strong reflection can be seen in **Figure 11**. Therefore we assume the fuselage echo to be the only aircraft structure reflection. For the implementation its bandwidth has to be determined.

Since the bandwidth of the fuselage echo is extremely small the ISIS algorithm is not able to estimate it. To

further investigate the fuselage process, we performed the following simulation:

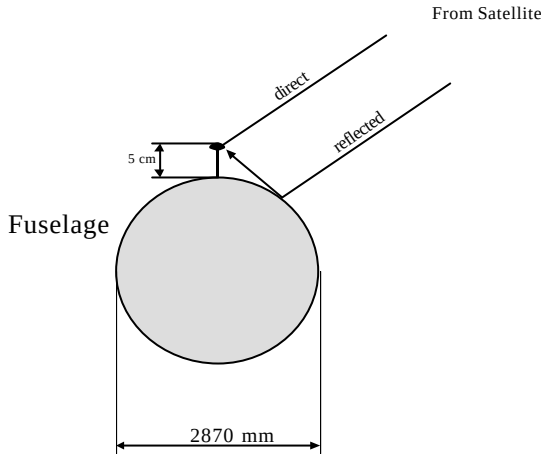

Figure 12: Simulating the fuselage echo

During the flight the experimental jet ATTAS recorded its movements. We used the measured roll, yaw and pitch data to model the aircrafts orientation in the air. During the final approach roll, pitch and

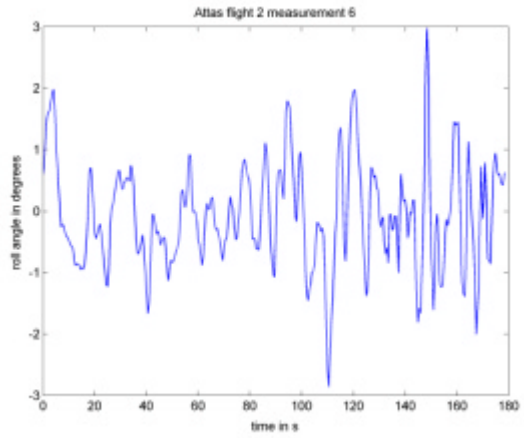

Figure 13: Roll angle

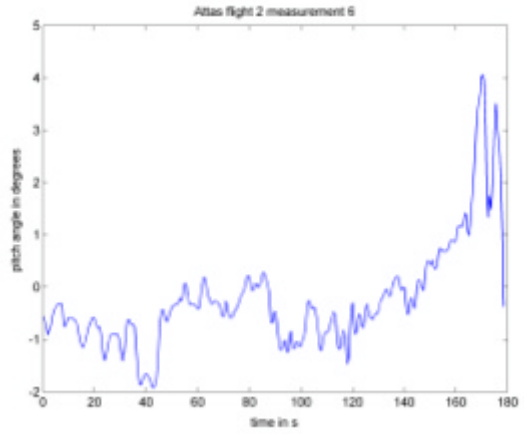

Figure 14: Pitch angle

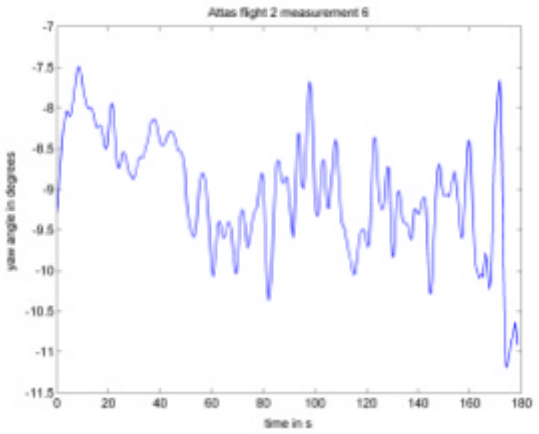

Figure 15: Yaw angle

yaw angles were recorded on the ATTAS as can be seen in **Figure 13** to **Figure 15**. For the aircrafts fuselage a simple cylinder model was used. For the ATTAS a mean fuselage radius of r = 1.435 m and an antenna height of 5 cm (as during the measurements) was taken for the model. We assumed an infinite far satellite, therefore we have parallel incoming signals for our model. Now we calculated the reflection points on the surface as the elevation and azimuth slightly changes during the landing. For each data point the angle of arrival was varied according to the flight data by rotating the cylinder model with its antenna. So for each time instance the reflection point on the cylinder and the excess length of the reflected ray, which is proportional to its relative phase, is calculated by

$$s(t)_{rec} = s(t) * \exp\left(-j\frac{2p \cdot \Delta s}{l}\right)$$

where Δs is the distance change and l is the wavelength.

This time variant phase shift causes a parasitic phase modulation. From this process, compared to the direct path, we obtained the following spectrum, as an example for 15° elevation and 75° azimuth (satellite position) in **Figure 16**. This spectrum shows, that there is a very strong constant (DC) component overlaid by a noisy process (fuselage process). The fuselage process can be approximated very well by an exponential function by using non-linear regression. The result is shown as well in the examples. The fuselage process is shown only up to a bandwidth of 2 Hz since the recorded ATTAS flight data was sampled at 2 Hz. Analysis of the fuselage reflections identified in the ISIS estimated power delay profile indicate that this exponential spectrum has a significant larger bandwidth.

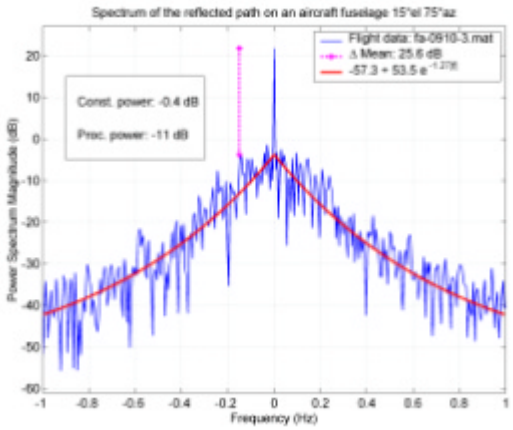

Figure 16: Fuselage echo spectrum

From this simulation we also got the already mentioned modulation of the direct path, which we assumed to be very much correlated to the fuselage process due to the fact that they are very close in terms of delay. So for the final model we modulated also the direct path signal with this process.

To expand our fuselage process model for different elevation and azimuth angles of the incoming rays, we repeated the simulation for other elevations and azimuths (Fuselage Igloo Approach).

All these simulations were performed for the GPS L1 frequency of 1575.42 MHz. For the simulation the ATTAS roll, pitch and yaw data which had been recorded every 0.5 seconds were interpolated in order to not limit the bandwidth of the simulated fuselage echo. A quarter of an "igloo" was simulated for elevations and azimuths between 0 and 90 degrees in 5 degree steps. Azimuth 0 degrees points to the nose of the plane. For each data point of the igloo the angle of arrival was varied according to the flight data by rotating the cylinder model with its antenna.

Due to the fact that the airplanes fuselage is not a cylinder, the cylindrical model shows an accuracy limit for azimuths around 0 and 180 degrees. For this the igloo was limited to elevations from 10 to 70 degrees and azimuths between 20 and 90 degrees. The following figures show the simulation results for the parameters mean, b_2 and b_3 of the fuselage echo spectrum, where b_2 and b_3 are the coefficients of the exponential process:

$$p_{proc}(dB) = k + b_2 \cdot e^{b_3|f|}$$

Please note that the total power of this process had been measured to be –14.2 dB which determines the constant

$$k = -14.2 - mean \quad [dB]$$

in the end. The smallest inner circle is 75 degree elevation and the largest on the outside gives the values for 5 degree elevation. The azimuth varies from 15 to 165 and 195 to 335 degrees respectively.

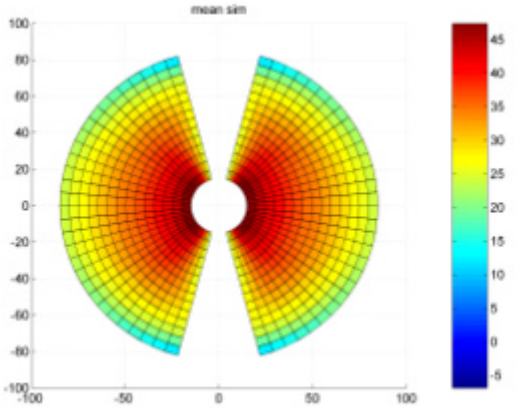

Figure 17: ATTAS parameter mean (DC component) - from fuselage simulation

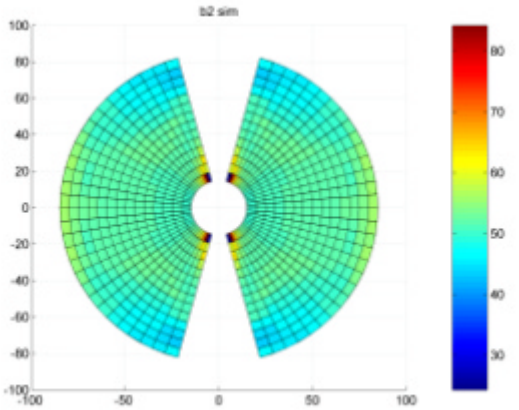

Figure 18: ATTAS parameter b_2 - from fuselage simulation

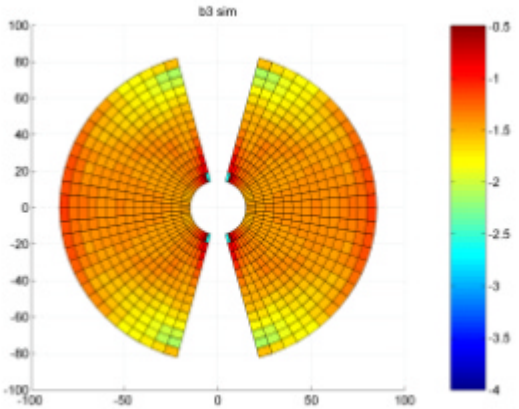

Figure 19: ATTAS parameter b_3 - from fuselage simulation

This simulation shows that the fuselage characteristics change very little by increasing the fuselage radius.

Figure 17 to **Figure 19** show the elevation and azimuth dependency of the fuselage reflection for the ATTAS. The mean value clearly decreases as the elevation decreases, that is because the variation in the fuselage reflection is higher due to the movement of the plane, which is mainly a rotation around the roll axis. We can also see that the mean value is smaller if the satellite is in front or in the rear of the plane.
The scaling factor for the exponential part of the fuselage spectrum b2 does not vary much. It is a little bit higher if the satellite is at the side of the airplane. More significant is the behaviour of the exponent b3. This parameter is highest for low elevations and azimuth directions front and rear. That means, for this situation the bandwidth is larger and therefore less critical compared to a satellite at high elevations at the side of the plane.
When we compare these results to the simulation of the Airbus with its larger fuselage radius, we can e.g. see that the mean value is even smaller at low elevations. There is more variation and therefore a larger bandwidth. The parameters are very similar to the results of the ATTAS simulation. Over all, the fuselage reflection seems to have a slightly larger bandwidth for the Airbus. The values of the matrices are attached in the appendix of this paper.

GROUND REFLECTION

Figure 20 shows the impulse responses prior to touch down in a larger time scale to display the ground reflection. It can explicitly be seen that the ground reflection has a quite low power. It is varying between the different flights but can coarsely be estimated in a range of -15 to -25 dB.
The delay is dependent on the altitude and is varying between 900 and 10 ns.

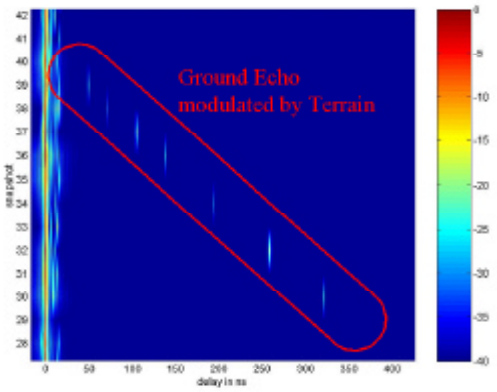

Figure 20: Flight 2_7 in a large time scale

For the ground reflection the Doppler spread is large enough for ISIS to estimate. We are now going to determine the spectrum of the ground reflection.

Figure 21 shows the cumulative spectrum of the ground reflection whilst landing.

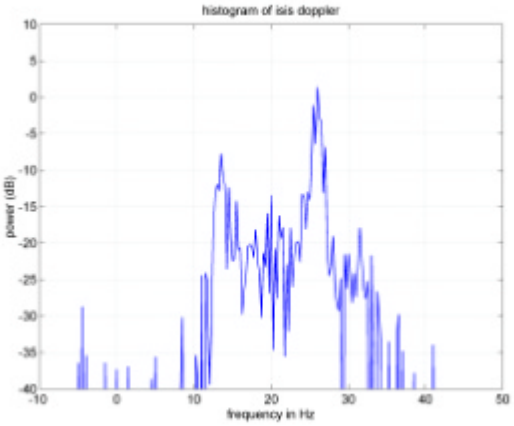

Figure 21: Cumulative spectrum of ISIS Doppler estimation

The desired descending speed was around 5 m/s, which is related to the strong components at 25 Hz. In the last phase of the approach, shortly before touch down, the descending speed decreases and, possibly from the runway, strong reflections can be seen between 10 and 20 Hz offset.

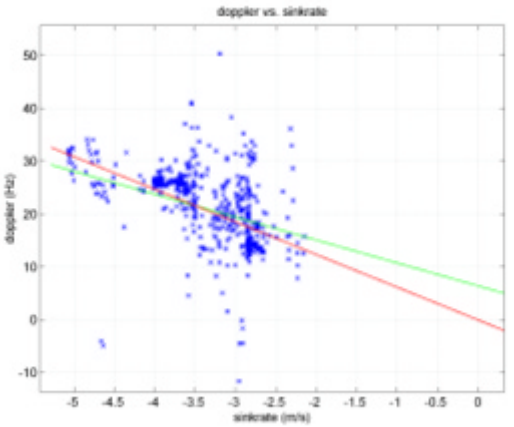

Figure 22: Doppler offset versus sink rate

Figure 22 gives the ISIS Doppler estimation as function of the actual sink rate during the whole landing approach. The green line indicates the linear regression of the data. It is obvious that the Doppler shift is related to the sink rate of the plane. Due to that the Doppler shift will be zero for a horizontally flying airplane. For this reason we force a zero crossing interpolation (red line) to give us the momentarily Doppler offset. A Doppler offset of approximately

6 Hz/(m/s) = 6 wavelengths/m ≈ 1/λ = 6,3 wavelengths/m. can be estimated. This finally proofs that the constant Doppler shift had been caused by the vertical speed.

Subtracting the Doppler offset from this data we plot the remaining power weighted ground reflection Doppler distribution of the approaching plane. **Figure 23** indicates that the bandwidth of the ground Doppler process is < 10 Hz.

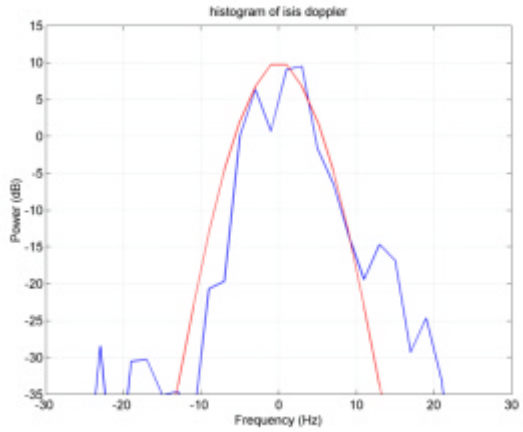

Figure 23: Doppler spectrum of ground reflection after vertical speed correction

Assuming a Gauss distributed ground reflection amplitude with zero mean, we can model the spectrum by

$$P_{Gr(dB)} = 20 * \log_{10}(k * e^{-\frac{f^2}{2s^2}})$$

where the deviation σ = 3.8 Hz is obtained as an average from flight 2 measurement 7 (σ = 3.66 Hz) and flight 3 measurement 6 (σ = 3.94 Hz). This model is indicated by the red line in **Figure 23** for flight 3 measurement 6.

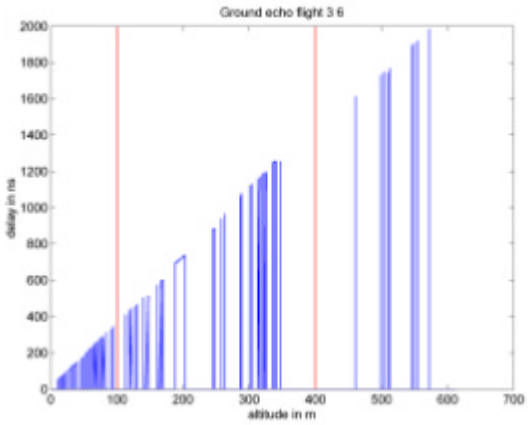

Figure 24: Altitude dependent ground echo occurrence

Please note that the Doppler bandwidth of 420 Hz in the old model [1] is significantly too high. For the implementation of the ground reflection model the parameter σ can be linearly scaled to the L1 frequency of 1575.42 MHz.

$$s_{L1} = \frac{f_{L1}}{f_{meas}} s = 3.0\,Hz$$

This concludes the definition of the Doppler process for the ground reflection.

Figure 24 shows the occurrence of the ground echo. It is quite obvious that the ground Echo is modulated by the reflecting terrain structure. To extract this process we divide the final approach into 3 different zones of altitude (high, mid and low altitude). In each zone the ground reflection is characterized by a Markov state model [6].

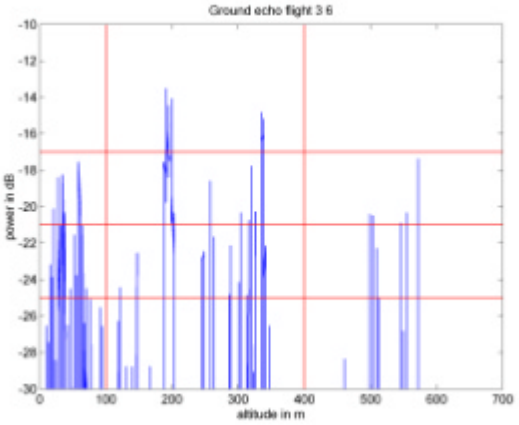

Figure 25: Power of ground reflection while descending.

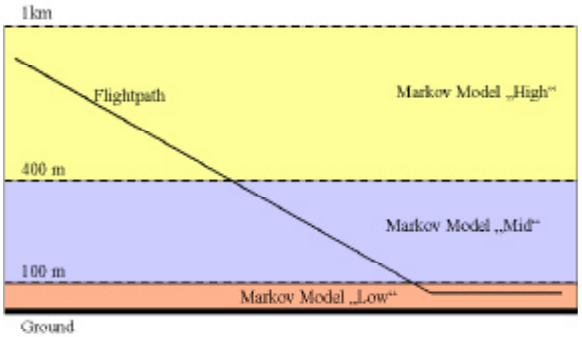

Figure 26: Altitude regions of the ground model

Furthermore we divided the occurring power levels in four power levels:

	Power in dB	Comment
State 1	-15 dB	
State 2	-19 dB	
State 3	-23 dB	
State 4	< -25 dB	“no ground reflection”

Table 2: States of the ground fading Markov model

Now we can obtain the Markov parameters from the quantised measurement data. The transition matrix P where $P_{x,y}$ is the probability of changing from state x to state y is determined for each altitude region independently.

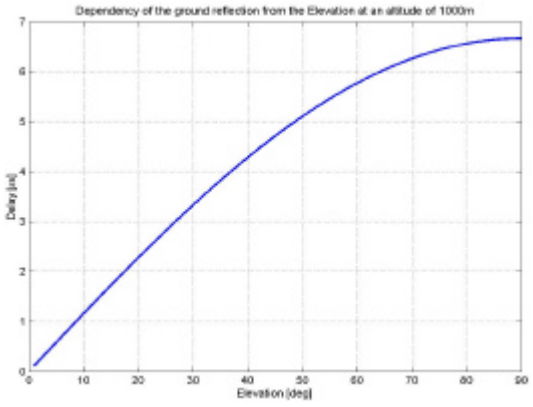

Figure 27: Ground delay dependency

The delay of the ground reflection as function of the elevation can be easily calculated assuming a flat environment around the airport by

$$t_{ground}(t) = \frac{2 \cdot h(t) \cdot \sin(e)}{C_0}$$

and is shown in **Figure 27** where h(t) is the current altitude and ε is the elevation angle.

MODEL

In contrast to the old “ESA-SDS” model (see **Table 1**) we obtained the following parameters from the measurements:

	Delay	Relative Power	Doppler BW
Refractive	0 ns	-14.2 dB	< 0.1 Hz
Fuselage	1.5 ns	-14.2 dB	< 0.1 Hz
Ground	900 – 10 ns (descending)	-15 to -25 dB	< 20 Hz biased due to sink rate

Table 3: The parameters of the new channel model - Overview

In this project we implemented the model in the “Channel State Generator” which can then be connected to a standard “Tapped Delay Line” (TDL) structure. This ensures the best portability of the model.

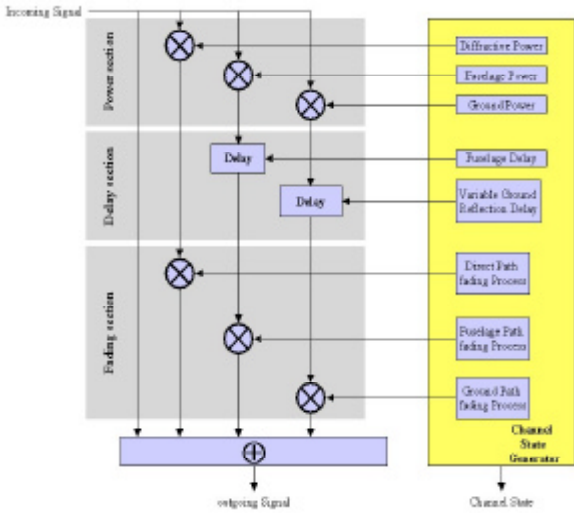

Figure 28: Realisation view of model

The complete Model is aimed to be used as a statistical simulator. Since the bandwidths of the reflections appear to be very low, the process will not show a sufficient statistics during the approach time of 200 s. To simulate a statistically satisfying navigation error, the model must be used for a large number of approaches. The simulation result of these approaches must be averaged to obtain the minimum, maximum and average navigation error.

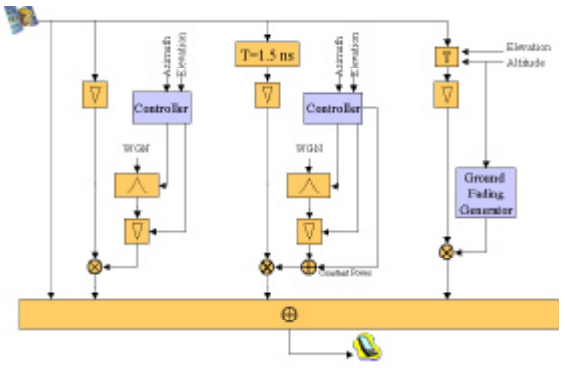

Figure 29: Complete aeronautical channel model

Figure 29 shows the complete aeronautical model for the final approach. The first branch is the direct signal, followed by the refractive part modelling the LOS modulation. The third branch consists of a 14.2 dB attenuated constant power overlaid by the fuselage process and delayed by 1.5 ns which models the fuselage echo. The last branch is the ground echo

whose delay depends on elevation and altitude. The fading processes and time variant blocks have input parameters for adjusting the model to different satellite positions (elevation and azimuth). Please note that the various fading processes are strongly dependent on the aircraft type.

For easier implementation of the fuselage reflection in the aeronautical model we fitted a 2-dimensional polynomial function of 4th order to each parameter (mean, b_2, b_3). As an example,

$$mean(e,j) = [\, e^4 \quad e^3 \quad e^2 \quad e \quad 1 \,] \cdot A_{mean} \cdot \begin{bmatrix} j^4 \\ j^3 \\ j^2 \\ j \\ 1 \end{bmatrix}$$

gives the mean value as function of elevation ε and azimuth φ, where A_{mean} is a 5-by-5 matrix of polynomial coefficients. The implemented model is valid for elevations between 10 and 70 degrees and azimuth from 20 to 160 and 200 to 340 degrees.

These matrices are given by:

$A_{mean,ATTAS} =$

-2.0057e-12	5.0499e-10	-4.6114e-8	1.8053e-6	-2.4773e-5
2.8598e-10	-7.4259e-8	7.0553e-6	-2.9116e-4	0.0043
-1.1568e-8	3.2474e-6	-3.3846e-4	0.0156	-0.2698
3.8681e-8	-2.2536e-5	0.0038	-0.2512	6.3140
1.9434e-6	-3.5747e-4	0.0133	0.8133	-28.1329

$A_{b3,ATTAS} =$

-1.8398e-12	4.2182e-10	-3.3813e-8	1.0855e-6	-1.0875e-5
2.6665e-10	-6.0897e-8	4.8490e-6	-1.5346e-4	0.0015
-1.2870e-8	2.9171e-6	-2.2947e-4	0.0071	-0.0629
2.3542e-7	-5.2520e-5	0.0040	-0.1193	0.9153
-1.2058e-6	2.5797e-4	-0.0187	0.5027	-4.1128

$A_{b2,ATTAS} =$

-3.9148e-11	8.8672e-9	-7.0048e-7	2.2069e-5	-2.1492e-4
6.0699e-9	-1.3708e-6	1.0784e-4	-0.0034	0.0322
-3.2203e-7	7.2344e-5	-0.0057	0.1747	-1.6206
6.7649e-6	-0.0015	0.1162	-3.5328	31.6814
-4.4741e-5	0.0098	-0.7383	21.9981	-142.3524

$A_{mean,A340} =$

-2.6220e-12	6.0886e-10	-5.0686e-8	1.8074e-6	-2.3633e-5
4.3848e-10	-1.0231e-7	8.6113e-6	-3.1465e-4	0.0044
-2.3577e-8	5.5538e-6	-4.7815e-4	0.0184	-0.2872
3.9552e-7	-9.2657e-5	0.0082	-0.3431	6.9937
-1.5225e-6	3.3690e-4	-0.0312	1.7110	-32.8066

$A_{b3,A340} =$

-1.2021e-12	2.7780e-10	-2.2626e-8	7.4413e-7	-7.5120e-6
1.7647e-10	-4.0725e-8	3.3131e-6	-1.0855e-4	0.0011
-8.6470e-9	1.9871e-6	-1.6099e-4	0.0052	-0.0488
1.6123e-7	-3.6656e-5	0.0029	-0.0946	0.8204
-8.5647e-7	1.8942e-4	-0.0149	0.4826	-5.5011

$A_{b2,A340} =$

-3.1880e-11	7.2724e-9	-5.8454e-7	1.9069e-5	-1.9707e-4
4.7229e-9	-1.0775e-6	8.6761e-5	-0.0028	0.0293
-2.3471e-7	5.3437e-5	-0.0043	0.1413	-1.4541
4.4756e-6	-0.0010	0.0812	-2.6731	27.5448
-2.5361e-5	0.0056	-0.4459	14.8917	-109.1083

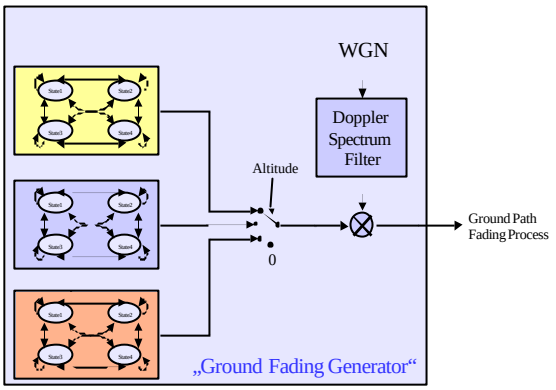

Figure 30: Realisation of the ground fading generator module

The ground fading process is generated by an altitude dependent Markov model for a sampling frequency of 25.4 Hz. Please note that these transition probabilities are only valid for this frequency. The transition altitudes are given

	From	To
Level “High”	1000 m	400 m
Level “Mid”	400 m	100 m
Level “Low”	100 m	0 m

Table 4: Altitude regions for the Markov model

The output power states of the model are depicted in **Table 2**.

From the measurements we obtained the following transition probability matrices:

$$P_{400-1500} = \begin{bmatrix} 0.9866 & 0.0087 & 0.0047 & 0 \\ 0.6087 & 0.3043 & 0.0870 & 0 \\ 0.2143 & 0.3571 & 0.4286 & 0 \\ 0.3333 & 0.3333 & 0.3334 & 0 \end{bmatrix}$$

$$P_{100-400} = \begin{bmatrix} 0.9842 & 0.0130 & 0.0028 & 0 \\ 0.6667 & 0.2222 & 0.0889 & 0.0222 \\ 0.0667 & 0.1167 & 0.5000 & 0.3166 \\ 0 & 0 & 0.3279 & 0.6721 \end{bmatrix}$$

$$P_{10-100} = \begin{bmatrix} 0.9645 & 0.0310 & 0.0045 & 0 \\ 0.7308 & 0.1538 & 0.1154 & 0 \\ 0.6250 & 0.1250 & 0.2500 & 0 \\ 0.3333 & 0.3333 & 0.3334 & 0 \end{bmatrix}$$

$$P_{0-10} = \begin{bmatrix} 1 & 0 & 0 & 0 \\ 1 & 0 & 0 & 0 \\ 1 & 0 & 0 & 0 \\ 1 & 0 & 0 & 0 \end{bmatrix}$$

Please note that this Markov model describes a very specific landing situation at Graz airport. Weather conditions, environment, flight geometry and many other parameters have influence on the characteristics of the ground echo.

CONCLUSION

We presented a high resolution aeronautical multipath model comprising detailed investigations on reflections on aircraft structures and ground reflections during final approach. Measurements and simulations show a strong reflection at the fuselage close to the antenna as the main contribution to the positioning error. We may safely assume that wing reflections are negligible and that echo bandwidths were assumed far too large in the past. And we were able to approve measurement results and simulation methods.

MODEL DOWNLOAD

The model will be offered for download. We refer to the following web sites:

http://www.dlr.de/kn/kn-s/steingass
http://www.dlr.de/kn/kn-s/lehner

AKNOWLEDGEMENTS

The work presented in this paper was carried out under a European Space Agency, ESA, contract entitled "Navigation signal measurement campaign for critical environments", by JOANNEUM RESEARCH (Austria) with subcontracts to DLR (Germany) and the University of Vigo (Spain).

REFERENCES

[1] R. Schweikert, T. Woerz. Signal design and transmission performance study for GNSS-2. Final Report, European Space Agency, 1998.

[2] Andreas Lehner, Alexander Steingaß, "The Influence of Multipath to Navigation Receivers", Global Navigation Satellite Systems Conference (GNSS2003), Graz, Austria

[3] Xuefeng Yin, Bernard H. Fleury, Patrik Jourdan and Andreas Stucki, “Doppler Frequency Estimation for Channel Sounding Using Switched Multiple Transmit and Receive Antennas”, GLOBECOM 2003, San Francisco, USA.

[4] W. L. Stutzman and G. A. Thiele Antenna Theory and design John Wiley, 1981.

[5] B.W. Parkinson, J.J. Spilker “Global Positioning System Theory and Applications I + II”, Volume 164 of Progress in Astronautics and Aeronautics. American Institute of Aeronautics and Astronautics Inc. Washington 1996.

[6] Athanasios Papoulis, “Probability, Random Variables and Stochastic Processes” Mc Graw-Hill Book Company, New York, 1965